# A Family of Inverting Buck-Boost Converters With Extended Conversion Ratios

## SHAN MIAO [ID] AND JINFENG GAO

School of Electrical Engineering, Zhengzhou University, Zhengzhou 450001, China

Corresponding author: Shan Miao (miaos@zzu.edu.cn)

**ABSTRACT** In this paper, two inverting buck-boost converters which possess wide conversion ratios are proposed. At the proper duty cycles, the inverting buck$^2$-boost converter (IB2BC) achieves high step-down gain while the inverting buck-boost$^2$ converter (IBB2C) realizes high step-up gain. Advantages of the IB2BC and the IBB2C also include fourth-order simple common-ground structures to increase the power density and operability, low components stress to decrease the corresponding losses and then to improve the system efficiency, no sudden changings on capacitors voltage to prevent the instantaneous overcurrent phenomenon. Owing to the special structures of the IB2BC and the IBB2C, their improved single-switch topologies with reduced number of switch and extensional topologies with wider conversion ratios are constructed, respectively. Operational principles and corresponding comparisons of the above mentioned buck-boost converters are deeply studied and analyzed. As the representative, the single-switch inverting buck-boost$^2$ converter (SIBB2C) is designed and experimented in step-down/up modes for verifying the family of buck-boost converters performance.

**INDEX TERMS** Buck-boost converters, inverting output voltage, single-switch converters, extended topologies, wide conversion ratio.

## I. INTRODUCTION

Applications such as renewable energy generation system, electric vehicle, portable electronic devices, light-emitting-diode lamps and so forth are in rapid development stage due to the enhancement of environmental awareness and usage requirements [1]–[3]. DC-DC converter plays an important part in these applications and the topology selection is an important factor influencing the system performance. According to the voltage bucking/boosting properties, DC-DC converters are classified into three kinds while the types of buck-boost converters can realize wider conversion ratios. Up to now, many species of buck-boost converters have already studied and applied.

The conventional buck-boost, Cuk, Sepic and Zeta converters can effectuate simple forms [4]. However, for the present applications, their limited conversion ratios make significant challenges for the improvement of efficiency and switching frequency, and also the realization of control circuit. By adjusting the turn ratio, coupled-inductor converters can realize wide conversion ratio in isolated or nonisolated situations. In [5], by combining the conventional

buck-boost converter with the coupled-inductor, the serious diode reverse recovery phenomenon is alleviated. Using the coupled-inductor technique, [6] presents a zero voltage switching buck-boost converter. But, auxiliary diodes are needed in these two topologies to generate recycle currents. Switched-network cells can be designed and applied to improve the performance of the conventional converters. In [7]–[11], inserting the cells which are formed by capacitors and semiconductors in the conventional converters, some new buck-boost converters are constructed. Combining the conventional converters with the switched-network cells which are composed of inductors and diodes, several kinds of modified converters are presented in [8] and [12]. In [13], [14], hybrid switched-network cell is embedded in the conventional Sepic and Cuk for constructing new converters. However, the aforementioned combined converters have complex structures and the increases of their conversion ratios are not obvious. In [15]–[17], three different kinds of buck-boost converters which are composed of the same number of semiconductors and energy storage components are presented. Unfortunately, these three converters' input and output terminals have no common-ground. To realize wide conversion ratio by only one switch, more capacitors and inductors are applied and then a series of buck-boost

The associate editor coordinating the review of this manuscript and approving it for publication was Meng Huang.
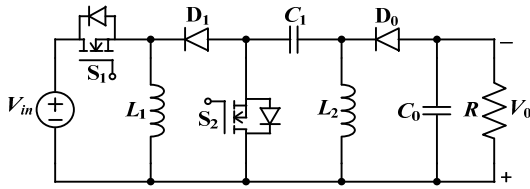
FIGURE 1. Topological structure of the IB2BC.



FIGURE 2. Topological structure of the IBB2C.

converters are analyzed in [18]–[21]. The additional energy storage elements make their converter structures complicated and increase the difficulty of modeling. In [22], several kinds of buck-boost converters and their isolated versions are presented. The conversion ratio $2D$ is realized in [23] by combining the synchronously rectified buck converter and the KY converter. In [24], a positive output polarity buck-boost converter which applies the interleaved strategy is presented. In [25], by cascading the modified versions of conventional converters, the topology of the new buck-boost converter is discussed and analyzed. In [26], through combining the conventional converters, a quadratic buck-boost converter is presented and researched. The aforementioned efforts try their best to improve the performance of the converters. Therefore, constructing powerful DC-DC converters, especially the buck-boost converters which realize the bucking/boosting voltage, is very important to broaden the family of buck-boost converters as well as to provide more possibilities for the industrial applications.

Here, in order to realize better performances, a series of inverting buck-boost converters are constructed in this paper. Without transformer or coupled inductor and at the proper duty cycles, the inverting buck$^2$-boost converter (IB2BC) and the inverting buck-boost$^2$ converter (IBB2C) achieve high step-down and high step-up gains, respectively. Besides, these two converters possess fourth-order simple common-ground structures to increase the power density and operability, low components stress to decrease the corresponding losses and then to improve the system efficiency, no sudden changings on capacitors voltage to prevent the instantaneous overcurrent phenomenon. What's more, owing to the special structures of the IB2BC and the IBB2C, their improved single-switch topologies and extensional topologies are constructed and analyzed, respectively.

The article organization is: the IB2BC and the IBB2C are analyzed in section II. In section III, their improved single-switch converters are constructed and studied. The extensional topologies are built and researched in section IV. Section V compares the converters performance. Related experiments are implemented in section VI to validate their effectiveness and feasibility. Section VII is the conclusions.

## II. OPERATIONAL PRINCIPLES AND ANALYSES
Fig. 1 and Fig. 2 show the topological structures of the IB2BC and the IBB2C, respectively. Of the two converters, $S_1$ and $S_2$ operate synchronously. $L_1$ and $L_2$ are magnetized
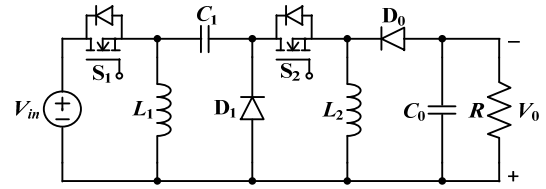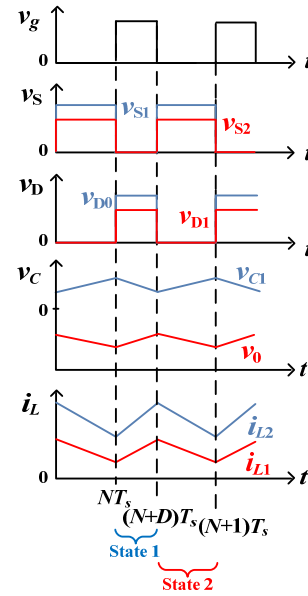


FIGURE 3. Main waveforms of the IB2BC.

while $C_1$ and $C_0$ are discharged when the switches on. Conversely, $L_1$ and $L_2$ are demagnetized while $C_1$ and $C_0$ are charged when the switches off.

The following are the operational principles of the IB2BC and the IBB2C in continuous conduction mode (CCM).

### A. ANALYSES OF THE IB2BC
In CCM, owing to the IB2BC has two synchronously controlled switches, hence state 1 and state 2 will be presented to discuss its operational principles, respectively. Fig. 3 presents main waveforms of the IB2BC while Fig. 4 displays its corresponding equivalent circuits.

State 1: Combining Fig. 3 and Fig. 4(a), one can see that the driving signal is high level and two switches are on while two diodes in reverse biased states. During this time interval, $L_1$ is magnetized from $V_{in}$ via $S_1$, $L_2$ is magnetized from $C_1$ via $S_2$, $C_0$ releases energy to $R$.

State 2: Owing to the low level driving signal, two switches are off while two diodes in forward biased states in Fig. 4(b). $L_1$ releases energy to $C_1$, $C_0$ and $R$ via $D_1$ and $D_0$. $L_2$ releases energy to $C_0$ and $R$ via $D_0$.

Based on the aforementioned analyses of the IB2BC, Table 1 lists the corresponding equations of the inductors voltage and the capacitors current in state 1 and state 2, respectively.
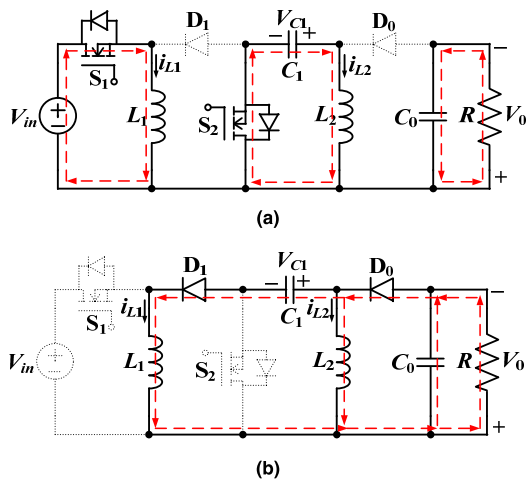
**FIGURE 4.** Equivalent circuits of the IB2BC. (a) State 1; (b) State 2.

**TABLE 1.** Equations of the IB2BC in state 1 and state 2.

| Parameters | State 1 | State 2 |
|---|---|---|
| $V_{L1}$ | $V_{in}$ | $-V_0 - V_{C1}$ |
| $V_{L2}$ | $V_{C1}$ | $-V_0$ |
| $I_{C1}$ | $-I_{L2}$ | $I_{L1}$ |
| $I_{C0}$ | $-I_0$ | $I_{L1} + I_{L2} - I_0$ |

**TABLE 2.** DC values of the IB2BC.

| Parameters | $V_{C1}$ | $V_{C0}$ | $I_{L1}$ | $I_{L2}$ |
|---|---|---|---|---|
| Values | $DV_{in}$ | $\dfrac{D^2}{1-D}V_{in}$ | $\dfrac{D}{1-D}I_0$ | $I_0$ |

Using the amp-second and volt-second balance principles for the IB2BC, DC values of its capacitors voltage and inductors current are got and presented in Table 2.

Also, it can be concluded that the conversion ratio of the IB2BC is

$$M = \frac{V_0}{V_{in}} = \frac{D^2}{1-D}. \tag{1}$$

From (1), one can see that the IB2BC possesses the voltage step-down property when $0 < D < 0.618$ and step-up property when $0.618 < D < 1$.

For the IB2BC, when the switches are on or the diodes in forward biased states, their current stress can be obtained separately. When the switches are off or the diodes in reverse biased states, the voltage stress on them can be obtained. Related current and voltage stress are displayed in Table 3.

**TABLE 3.** Related stress of the IB2BC.

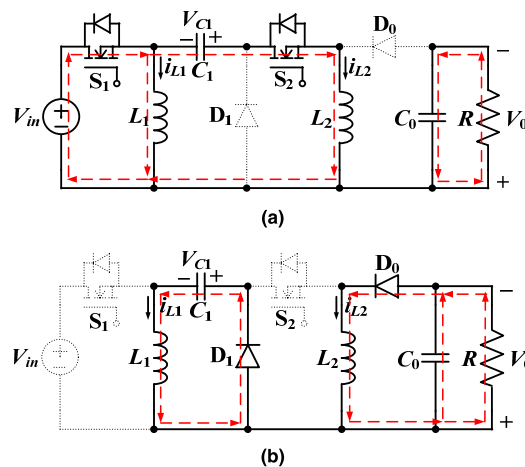| Parameters | Voltage Stress | Current Stress |
|---|---|---|
| $S_1$ | $V_{S1} = \dfrac{1}{1-D}V_{in}$ | $I_{S1} = \dfrac{D^2}{1-D}I_0$ |
| $S_2$ | $V_{S2} = \dfrac{D}{1-D}V_{in}$ | $I_{S2} = DI_0$ |
| $D_1$ | $V_{D1} = V_{in}$ | $I_{D1} = DI_0$ |
| $D_0$ | $V_{D0} = \dfrac{D}{1-D}V_{in}$ | $I_{D0} = I_0$ |



**FIGURE 5.** Equivalent circuits of the IBB2C. (a) State 1; (b) State 2.

## B. ANALYSES OF THE IBB2C

According to the status of $S_1$ and $S_2$, there are two states when the IBB2C operating in CCM. The main waveforms of the IBB2C are similar to that of the IB2BC and Fig. 5 presents the IBB2C's equivalent circuits.

State 1: As shown in Fig. 5(a), two switches are on while two diodes in reverse biased states in this state. $L_1$ is magnetized from $V_{in}$ via $S_1$, $L_2$ is magnetized from $V_{in}$ and $C_1$ via $S_1$ and $S_2$, $C_0$ releases energy to $R$.

State 2: In this state, two switches are off while two diodes in forward biased states, as shown in Fig. 5(b). $L_1$ releases energy to $C_1$ via $D_1$, $L_2$ releases energy to $C_0$ and $R$ via $D_0$.

Combining the operational principles of the above mentioned two states, the corresponding equations of the inductors voltage and capacitors current of the IBB2C are given out in Table 4.

Similarly, applying the amp-second and volt-second balance principles, Table 5 presents the derived DC values of the IBB2C.

Therefore, the conversion ratio of the IBB2C can be obtained as

$$M = \frac{V_0}{V_{in}} = \frac{D}{(1-D)^2}. \tag{2}$$

**TABLE 4.** Equations of the IBB2C in state 1 and state 2.

| Parameters | State 1 | State 2 |
|---|---|---|
| $V_{L1}$ | $V_{in}$ | $-V_{C1}$ |
| $V_{L2}$ | $V_{in} + V_{C1}$ | $-V_0$ |
| $I_{C1}$ | $-I_{L2}$ | $I_{L1}$ |
| $I_{C0}$ | $-I_0$ | $I_{L2} - I_0$ |

**TABLE 5.** DC values of the IBB2C.

| Parameters | $V_{C1}$ | $V_{C0}$ | $I_{L1}$ | $I_{L2}$ |
|---|---|---|---|---|
| Values | $\dfrac{D}{1-D}V_{in}$ | $\dfrac{D}{(1-D)^2}V_{in}$ | $\dfrac{D}{(1-D)^2}I_0$ | $\dfrac{1}{1-D}I_0$ |

**TABLE 6.** Related stress of the IBB2C.

| Parameters | Voltage Stress | Current Stress |
|---|---|---|
| $S_1$ | $V_{S1} = \dfrac{1}{1-D}V_{in}$ | $I_{S1} = \dfrac{D}{(1-D)^2}I_0$ |
| $S_2$ | $V_{S2} = \dfrac{D}{(1-D)^2}V_{in}$ | $I_{S2} = \dfrac{D}{1-D}I_0$ |
| $D_1$ | $V_{D1} = \dfrac{1}{1-D}V_{in}$ | $I_{D1} = \dfrac{D}{1-D}I_0$ |
| $D_0$ | $V_{D0} = \dfrac{1}{(1-D)^2}V_{in}$ | $I_{D0} = I_0$ |

It can be concluded that $M = 1$ when $D = 0.382$. Therefore, for the IBB2C, the step-down gain is obtained when $0 < D < 0.382$ and the step-up gain is achieved when $0.382 < D < 1$.

The voltage stress on $S_1$, $S_2$, $D_1$, $D_0$ when they are off and the current stress through $S_1$, $S_2$, $D_1$, $D_0$ when they are on are calculated and shown in Table 6.

## III. SINGLE-SWITCH CONVERTERS

Compared with the two or more switches converters, their improved single-switch converter can ameliorate the power density and reliability; reduce the losses, cost and driving circuit complexity. The IB2BC and the IBB2C possess the special structures that their synchronously controlled switches have the common node. Therefore, by the graft scheme, they can be converted to the single-switch forms [27].

The topological structures of the single-switch inverting buck$^2$-boost converter (SIB2BC) and the single-switch inverting buck-boost$^2$ converter (SIBB2C) are displayed in Fig. 6(a) and (b), respectively. Next, they will be deeply analyzed as follows.
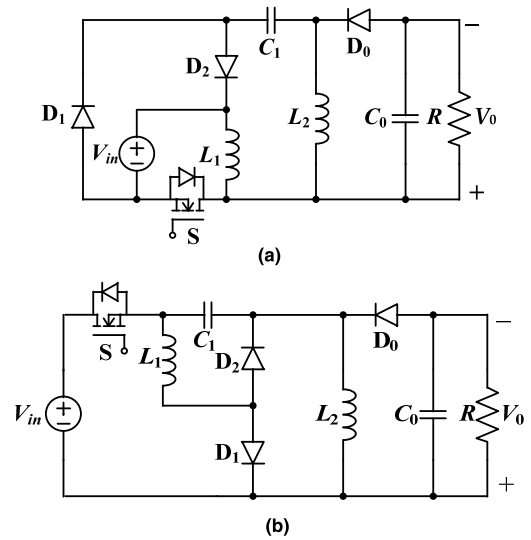


**FIGURE 6.** Topological structures of the improved single-switch converters. (a) SIB2BC; (b) SIBB2C.
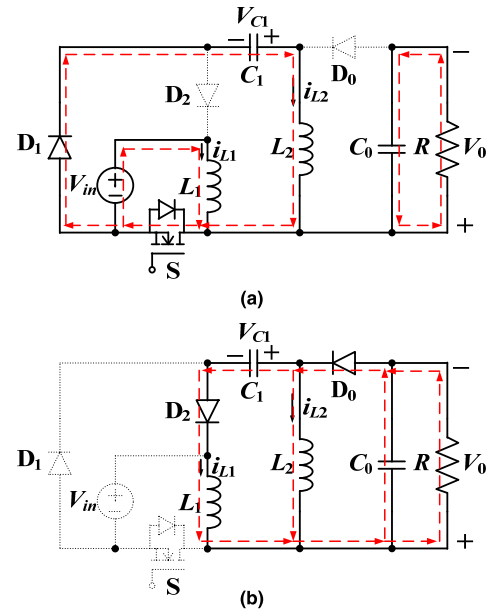


**FIGURE 7.** Equivalent circuits of the SIB2BC. (a) State 1; (b) State 2.

### A. ANALYSES OF THE SIB2BC

The SIB2BC has two states in CCM. Fig. 7(a) shows that the SIB2BC operates in state 1 and Fig. 7(b) reveals the operations in state 2.

State 1: As shown in Fig. 7(a), the switch is on in this time interval, the diode $D_1$ in forward biased state while the diodes $D_2$ and $D_0$ in reverse biased states. $L_1$ is magnetized from $V_{in}$ via S, $L_2$ is magnetized from $C_1$ via S and $D_1$, $C_0$ releases energy to R.

State 2: The equivalent circuit of this state is shown in Fig. 7(b), the switch is off, the diode $D_1$ in reverse biased state, the diodes $D_2$ and $D_0$ in forward biased states. $L_1$ releases energy to $C_1$, $C_0$ and R via $D_2$ and $D_0$. $L_2$ releases energy to $C_0$ and R via $D_0$.

**TABLE 7.** Related stress of the SIB2BC.

| Parameters | Voltage Stress | Current Stress |
|---|---|---|
| S | $V_S = \dfrac{1}{1-D}V_{in}$ | $I_S = \dfrac{D}{1-D}I_0$ |
| $D_1$ | $V_{D1} = V_{in}$ | $I_{D1} = DI_0$ |
| $D_2$ | $V_{D2} = V_{in}$ | $I_{D2} = DI_0$ |
| $D_0$ | $V_{D0} = \dfrac{D}{1-D}V_{in}$ | $I_{D0} = I_0$ |

**TABLE 8.** Related stress of the SIBB2C.

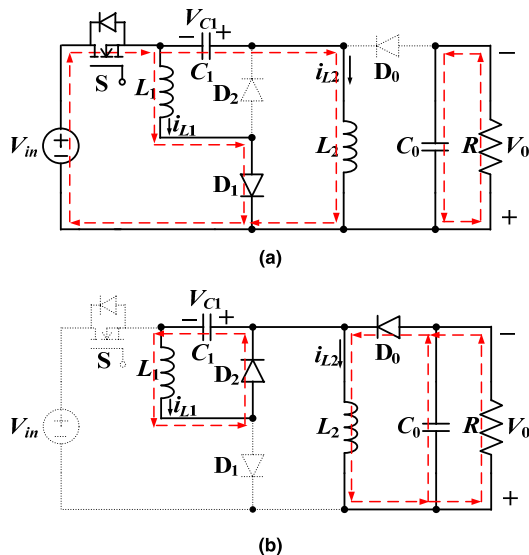| Parameters | Voltage Stress | Current Stress |
|---|---|---|
| S | $V_S = \dfrac{1}{(1-D)^2}V_{in}$ | $I_S = \dfrac{D}{(1-D)^2}I_0$ |
| $D_1$ | $V_{D1} = \dfrac{D}{(1-D)^2}V_{in}$ | $I_{D1} = \dfrac{D^2}{(1-D)^2}I_0$ |
| $D_2$ | $V_{D2} = \dfrac{1}{1-D}V_{in}$ | $I_{D2} = \dfrac{D}{1-D}I_0$ |
| $D_0$ | $V_{D0} = \dfrac{1}{(1-D)^2}V_{in}$ | $I_{D0} = I_0$ |



**FIGURE 8.** Equivalent circuits of the SIBB2C. (a) State 1; (b) State 2.

By comparing the components number and the operational principles of the SIB2BC and the IB2BC, it is seen that these two converters possess the same number of energy storage elements while the former has reduced number of switch. Owing to the energy transform processes of these two converters are the same, the SIB2BC and the IB2BC possess the same DC values and conversion ratio. Table 7 shows the related stress of the SIB2BC.

### B. ANALYSES OF THE SIBB2C

Fig. 8 draws the equivalent circuits of the SIBB2C in CCM and the detailed analyses are presented as follows.

State 1: The switch is on in this state and the diode $D_1$ in forward biased mode. The diodes $D_2$ and $D_0$ in reverse biased states, as shown in Fig. 8(a). $L_1$ is magnetized from $V_{in}$ via S and $D_1$, $L_2$ is magnetized form $V_{in}$ and $C_1$ via S, $C_0$ releases energy to $R$.

State 2: Within this time interval, the switch is off, the diode $D_1$ in reverse biased state, the diodes $D_2$ and $D_0$ in forward biased states, as shown in Fig. 8(b). $L_1$ releases energy to $C_1$ via $D_2$, $L_2$ releases energy to $C_0$ and $R$ via $D_0$.

The similarly operational principles make that the SIBB2C and the IBB2C have the same conversion ratio. Besides,

these two converters possess the same number of energy storage elements while the former has reduced number of switch. Table 8 lists the corresponding stress of the SIBB2C within the whole operating range.

## IV. EXTENDED TOPOLOGIES

In order to realize higher step-down/up gains for the applications that wider conversion ranges are needed, the extended topologies of the inverting buck$^2$-boost converter (EIB2BC) and the extended topologies of the inverting buck-boost$^2$ converter (EIBB2C) are constructed and analyzed as follows.

### A. ANALYSES OF THE EIB2BC

The mid-structure of the IB2BC is a cell of switched network which is composed of "$L$-D-S-$C$". Combining "$n$" cells of "$L$-D-S-$C$" structures with the IB2BC, as shown in Fig. 9, we can obtain the topological structure of the EIB2BC.

The EIB2BC possesses "$n+2$" switches, "$n+2$" diodes, "$n+2$" inductors, "$n+2$" capacitors and one load. When the driving signal is high level, the switches are on synchronously, the diodes in reverse biased states, the inductors magnetized and the capacitors discharged. Otherwise, the components operate conversely.

The conversion ratio of the EIB2BC is derived as follows:

$$M = \frac{V_0}{V_{in}} = \frac{D^{n+2}}{1-D}. \tag{3}$$

Based on (3), with the switched network number $n = 2$, the boundary duty cycle between bucking and boosting of the EIB2BC can be deduced as 0.725.

### B. ANALYSES OF THE EIBB2C

From Fig. 2, we can see that the mid-structure of the IBB2C is a switched-network cell which consists of "$C$-D-S-$L$". Similarly, combining "$n$" cells of "$C$-D-S-$L$" structures with the IBB2C, the topological structure of the EIBB2C can be obtained and shown in Fig. 10. The EIBB2C is a "$2n+4$" order circuit with "$n+2$" synchronously controlled switches.

The CCM gain of the EIBB2C is:

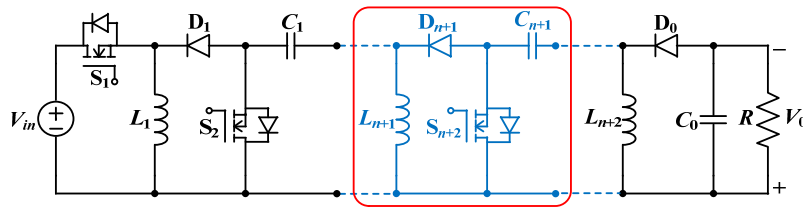$$M = \frac{V_0}{V_{in}} = \frac{D}{(1-D)^{n+2}}. \tag{4}$$

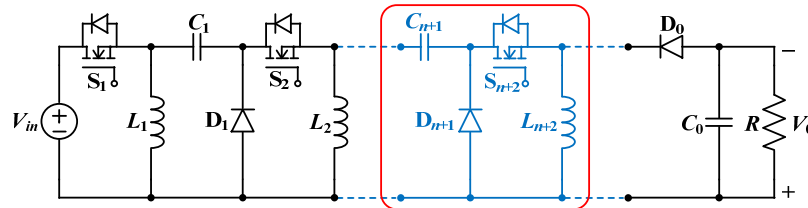**FIGURE 9.** Topological structure of the EIB2BC.



**FIGURE 10.** Topological structure of the EIBB2C.

**TABLE 9.** Performance comparisons.

| Types | Conventional buck-boost converter | Buck-boost converter in [10] | Buck-boost converter in [25] | Buck-boost converter in [26] | IB2BC | IBB2C |
|---|---|---|---|---|---|---|
| No. of S/D/L/C | 1/1/1/1 | 1/2/3/4 | 2/2/2/2 | 1/5/3/3 | 2/2/2/2 | 2/2/2/2 |
| Conversion Ratio | $M = \dfrac{D}{1-D}$ | $M = \dfrac{2D}{1-D}$ | $M = \dfrac{D}{(1-D)^2}$ | $M = \dfrac{D^2}{(1-D)^2}$ | $M = \dfrac{D^2}{1-D}$ | $M = \dfrac{D}{(1-D)^2}$ |
| Switches Voltage Stress | $V_S = \dfrac{1}{1-D}V_{in}$ | $V_S = \dfrac{1}{1-D}V_{in}$ | $V_{S1} = \dfrac{1}{1-D}V_{in}$ $V_{S2} = \dfrac{D}{(1-D)^2}V_{in}$ | $V_S = \dfrac{1}{(1-D)^2}V_{in}$ | $V_{S1} = \dfrac{1}{1-D}V_{in}$ $V_{S2} = \dfrac{D}{1-D}V_{in}$ | $V_{S1} = \dfrac{1}{1-D}V_{in}$ $V_{S2} = \dfrac{D}{(1-D)^2}V_{in}$ |
| Inverting output voltage | Yes | No | Yes | Yes | Yes | Yes |
| Common -ground | Yes | No | Yes | Yes | Yes | Yes |

In the condition $n = 2$, one can get that the EIBB2C achieves $D = 0.275$ when $M = 1$. The boundary duty cycle of the EIBB2C with $n = 2$ is smaller than that of the IBB2C, so the EIBB2C possess higher step-up gain.

## V. COMPARISONS AMONG CONVERTERS
Here, performance comparisons are made among the canonical and proposed buck-boost converters as follows. Table 9 displays the comparisons about number of components, conversion ratio, switches voltage stress, output voltage polarity and property of common-ground in detail. Meanwhile, their conversion ratios versus duty cycle are drawn in Fig. 11 and one can see that the IB2BC has the highest step-down gain while the IBB2C has the highest step-up gain.

By comparing the stress of the aforementioned buck-boost converters, one can see that the IB2BC and the IBB2C possess low switches voltage stress. What's more,
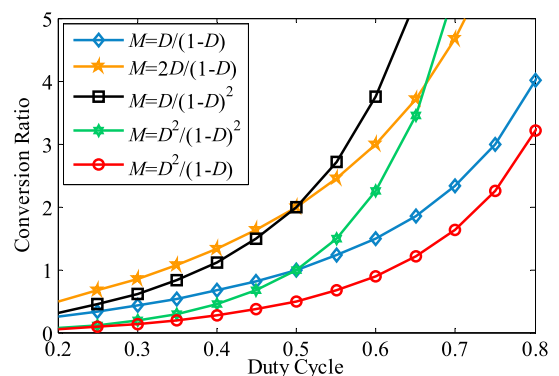


**FIGURE 11.** Comparisons about the conversion ratios versus the duty cycle.

the IBB2C and the buck-boost converter in [25] have the similar presented performance while the former possesses reduced mid-capacitor voltage. Features of the proposed
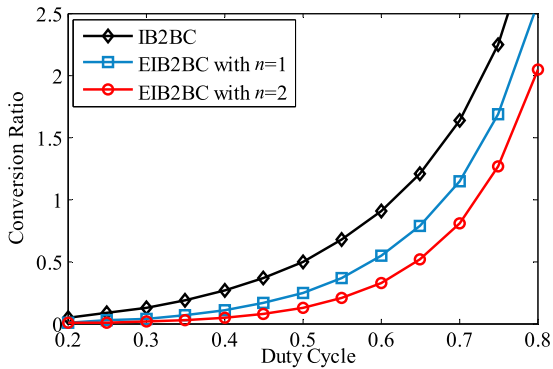
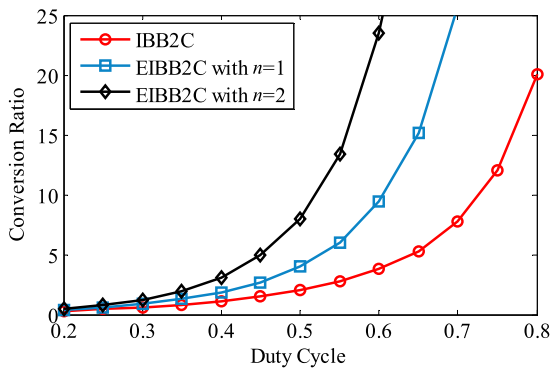**FIGURE 12.** Conversion ratio comparisons among the IB2BC and the EIB2BC.



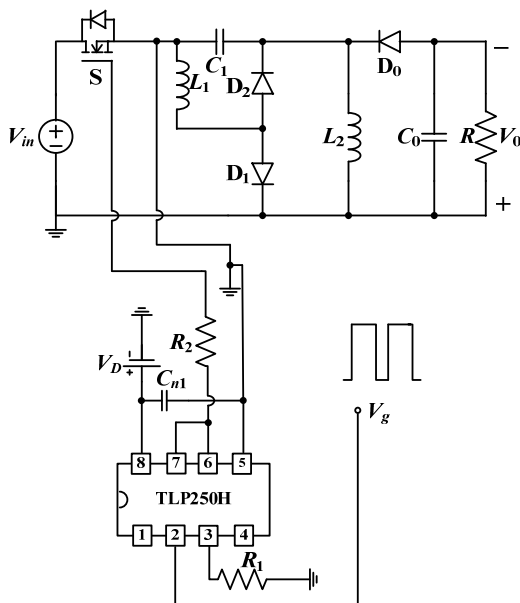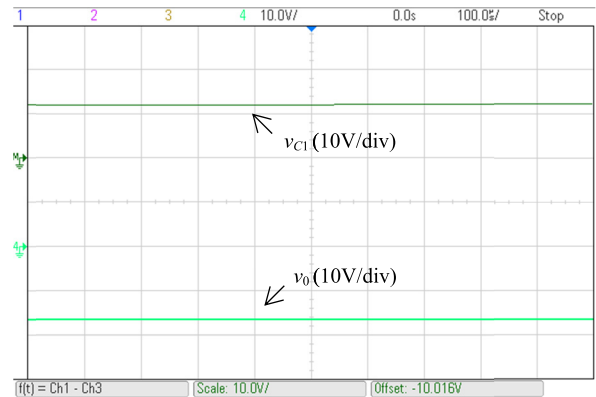**FIGURE 13.** Conversion ratio comparisons among the IBB2C and the EIBB2C.



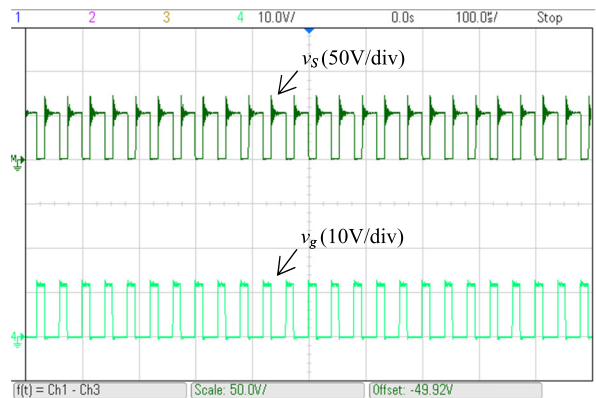**FIGURE 14.** Experimental schematic diagram of the SIBB2C.



**FIGURE 15.** Experimental results of the SIB2C in step-down mode. (a) $v_{C1}$ and $v_0$. (b) $v_S$ and $v_g$.

buck-boost converters are benefit for decreasing the component losses and then improving the efficiency.

When switches are on, the mid-capacitors of the IB2BC and the IBB2C constitutes a closed-loop with inductors, not a direct connection only with the input voltage, in result that

their capacitors voltage cannot be suddenly changed and the instantaneous overcurrent is prevented.

After the above comparisons, it is concluded that the IB2BC and the IBB2C possess better performance.

The analyses about the IB2BC and the SIB2C, the IBB2C and the SIBB2C demonstrate that the improved single-switch converters can ameliorate the power density and reliability; reduce the losses, cost and driving circuit complexity.

The comparisons between the IB2BC and the EIB2BC are shown in Fig. 12. With $D = 0.4$ which is far away from the extreme duty cycle, the conversion ratios of the IB2BC, EIB2BC with $n = 1$ and $n = 2$ are 0.267, 0.107 and 0.043, respectively. Hence, the EIB2BC possesses higher step-down gain. With more switched network cells applied, the EIB2BC can improve the conversion ratio significantly.

Similarly, the conversion ratios versus different duty cycle of the IBB2C, the EIBB2C with $n = 1$ and $n = 2$ are displayed in Fig. 13. From Fig. 13, we can see that at a proper duty cycle $D = 0.6$, the conversion ratios of these three converters are 3.75, 9.38 and 23.44, respectively. That is to say, the extended topologies possess higher voltage boosting property. With more switched network cells used in the EIBB2C, higher conversion ratio can be realized.
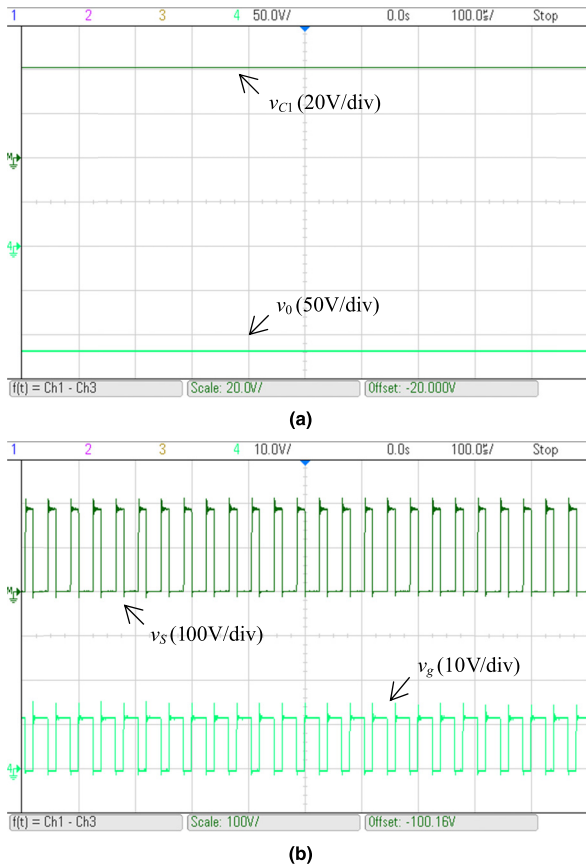
(a)



(b)

**FIGURE 16.** Step-up mode experimental results of the SIBB2C. (a) $v_{C1}$ and $v_0$. (b) $v_S$ and $v_g$.

## VI. EXPERIMENTAL VERIFICATION

Based on the aforementioned analyses, the SIBB2C is implemented in the laboratory as an example to verify their operability and feasibility. Selections of components are IRFP264N ($V_{DSS} = 250$V, $r_{DS}$(on) $= 60$m $\Omega$) for switch S, MUR820 ($V_{RRM} = 200$V, $V_F = 0.975$V) for diodes $D_1$ and $D_0$, MUR810 ($V_{RRM} = 100$V, $V_F = 0.975$V) for diode $D_2$, $L_1 = 470\mu$H, $L_2 = 2.2$mH, $C_1 = 30\mu$F and $C_0 = 30\mu$F. The experimental schematic diagram of the SIBB2C is drawn in Fig. 14. It must be noted that the photocoupler TLP250H is adopted here to produce the isolated driving signal for the floating switch S.

### A. STEP-DOWN MODE EXPERIMENTAL RESULTS

Applying the circuit selections above and setting $V_{in} = 24$V, $f_s = 25$kHz, $D = 0.34$, $R = 14\Omega$. The experimental time-domain waveforms can be obtained and displayed in Fig. 15. In Fig. 15(a), from top to bottom are the mid-capacitor voltage $v_{C1}$ (12V) and the output voltage $v_0$ ($-18$V). In Fig. 15(b), from top to bottom are the switch voltage stress $v_S$ (55V) and the driving signal $v_g$.

Combining the calculations and the experiments, it is clear that these two have consistent results, which prove the correctness of the researches and discusses in step-down mode.
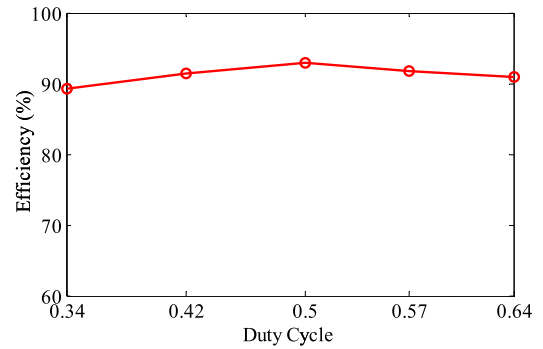


**FIGURE 17.** Efficiency of the SIBB2C versus the duty cycle.

### B. STEP-UP MODE EXPERIMENTAL RESULTS

For verifying the SIBB2C properties in step-up mode, the parameters aforementioned and the diagram in Fig. 14 are applied. Other presuppositions are $V_{in} = 24$V, $D = 0.64$, $R = 550\Omega$ and $f_s = 25$kHz in this part. The measured waveforms in Fig. 16(a) are the mid-capacitor voltage $v_{C1}$(42V) and the output voltage $v_0$ ($-118$V), in Fig. 16(b) are the switch voltage stress $v_S$ (185V) and the driving signal $v_g$.

Comparing the experiments with the analyses, one can see that these two results are consisting with each other in step-up mode.

### C. EFFICIENCY

When $D$ varies from 0.34 to 0.64, the experimental efficiencies of the SIBB2C are drawn in Fig. 17, one can see that efficiencies of the SIBB2C are up to 90%. Besides the components losses, the losses on wires, contact points and the driving circuits are also occurred in hardware experiments.

The above mentioned experimental time-domain waveforms and efficiencies of the SIBB2C effectively proved the proposed converter topologies' feasibility and maneuverability.

## VII. CONCLUSION

Here, a family of buck-boost converters which possess inverting output polarity and wide conversion ratio is proposed and analyzed. The IB2BC realizes high step-down gain while the IBB2C obtains high step-up gain. Besides, these two converters have simple common-ground topological structures, low voltage and current stress, and no sudden changings on capacitors voltage. What's more, owing to the special structures of the IB2BC and the IBB2C, their improved single-switch topologies and extensional topologies are constructed and studied, respectively. Based on the theoretical analyses and performance comparisons, the SIBB2C is designed and experimented as the representative for verifying the performance of the proposed converter topologies. Hence, this proposed family of the inverting buck-boost converters satisfies current requirements and future switching-mode power supply trends, and can be applied to wide conversion range applications.

## REFERENCES

[1] W. Li and X. He, "Review of nonisolated high-step-up DC/DC converters in photovoltaic grid-connected applications," *IEEE Trans. Ind. Electron.*, vol. 58, no. 4, pp. 1239–1250, Apr. 2011.

[2] V. Samavatian and A. Radan, "A high efficiency input/output magnetically coupled interleaved buck–boost converter with low internal oscillation for fuel-cell applications: CCM steady-state analysis," *IEEE Trans. Ind. Electron.*, vol. 62, no. 9, pp. 5560–5568, Sep. 2015.

[3] M. Forouzesh, Y. P. Siwakoti, S. A. Gorji, F. Blaabjerg, and B. Lehman, "Step-Up DC–DC converters: A comprehensive review of voltage-boosting techniques, topologies, and applications," *IEEE Trans. Power Electron.*, vol. 32, no. 12, pp. 9143–9178, Dec. 2017.

[4] T.-F. Wu and Y.-K. Chen, "Modeling PWM DC/DC converters out of basic converter units," *IEEE Trans. Power Electron.*, vol. 13, no. 5, pp. 870–881, Sep. 1998.

[5] C. Yang, S. Xie, L. Mao, and Z. Zhang, "Efficiency improvement on two-switch buck-boost converter with coupled inductor for high-voltage applications," *IET Power Electron.*, vol. 7, no. 11, pp. 2846–2856, Nov. 2014.

[6] X.-F. Cheng, Y. Zhang, and C. Yin, "A zero voltage switching topology for non-inverting buck–boost converter," *IEEE Trans. Circuits Syst., II, Exp. Briefs*, vol. 66, no. 9, pp. 1557–1561, Sep. 2019.

[7] E. H. Ismail, M. A. Al-Saffar, A. J. Sabzali, and A. A. Fardoun, "A family of single-switch PWM converters with high step-up conversion ratio," *IEEE Trans. Circuits Syst. I, Reg. Papers*, vol. 55, no. 4, pp. 1159–1171, May 2008.

[8] B. Axelrod, Y. Berkovich, and A. Ioinovici, "Switched-capacitor/switched-inductor structures for getting transformerless hybrid DC–DC PWM converters," *IEEE Trans. Circuits Syst. I, Reg. Papers*, vol. 55, no. 2, pp. 687–696, Mar. 2008.

[9] B. Axelrod, Y. Berkovich, S. Tapuchi, and A. Ioinovici, "Single-stage single-switch switched-capacitor buck/buck-boost-type converter," *IEEE Trans. Aerosp. Electron. Syst.*, vol. 45, no. 2, pp. 419–430, Apr. 2009.

[10] E. H. Ismail, A. A. Fardoun, and A. A. Zerai, "Step-up/step-down DC-DC converter with near zero input/output current ripples," *Int. J. Circuit Theory Appl.*, vol. 42, no. 4, pp. 358–375, 2014.

[11] M. Veerachary and V. Khubchandani, "Analysis, design, and control of switching capacitor based buck–boost converter," *IEEE Trans. Ind. Appl.*, vol. 55, no. 3, pp. 2845–2857, May/Jun. 2019.

[12] A. J. Sabzali, E. H. Ismail, M. A. Al-Saffar, and H. M. Behbehani, "Non-isolated single-switch DC-DC converters with extended duty cycle for high step-down voltage applications," *Int. J. Circuit Theory Appl.*, vol. 43, no. 8, pp. 1080–1094, 2015.

[13] B. Wang and W. Tang, "A new CUK-based Z-source inverter," *Electronics*, vol. 7, no. 11, p. 313, 2018.

[14] B. Wang and W. Tang, "A novel three-switch Z-source SEPIC inverter," *Electronics*, vol. 8, no. 2, p. 247, 2019.

[15] B. Moon, H. Y. Jung, S. H. Kim, and S.-H. Lee, "A modified topology of two-switch buck-boost converter," *IEEE Access*, vol. 5, pp. 17772–17780, 2004.

[16] H.-S. Son, J.-K. Kim, J.-B. Lee, S.-S. Moon, J.-H. Park, and S.-H. Lee, "A new buck–boost converter with low-voltage stress and reduced conducting components," *IEEE Trans. Ind. Electron.*, vol. 64, no. 9, pp. 7030–7038, Sep. 2017.

[17] H. Y. Jung, S. H. Kim, B. Moon, and S.-H. Lee, "A new circuit design of two-switch buck-boost converter," *IEEE Access*, vol. 6, pp. 47415–47423, 2018.

[18] A. Ajami, H. Ardi, and A. Farakhor, "Design, analysis and implementation of a buck–boost DC/DC converter," *IET Power Electron.*, vol. 7, no. 12, pp. 2902–2913, Dec. 2014.

[19] M. R. Banaei and H. A. F. Bonab, "A novel structure for single-switch nonisolated transformerless buck–boost DC–DC converter," *IEEE Trans. Ind. Electron.*, vol. 64, no. 1, pp. 198–205, Jan. 2017.

[20] M. R. Banaei and H. A. F. Bonab, "High-efficiency transformerless buck–boost DC–DC converter," *Int. J. Circuit Theory Appl.*, vol. 45, no. 8, pp. 1129–1150, 2017.

[21] M. R. Banaei and S. G. Sani, "Analysis and implementation of a new SEPIC-based single-switch buck–boost DC–DC converter with continuous input current," *IEEE Trans. Power Electron.*, vol. 33, no. 12, pp. 10317–10325, Dec. 2018.

[22] D. Maksimovic and S. Cuk, "Switching converters with wide DC conversion range," *IEEE Trans. Power Electron.*, vol. 6, no. 1, pp. 151–157, Jan. 1991.

[23] K. I. Hwu and T. J. Peng, "A novel buck–boost converter combining KY and buck converters," *IEEE Trans. Power Electron.*, vol. 27, no. 5, pp. 2236–2241, May 2012.

[24] H.-K. Liao, T.-J. Liang, L.-S. Yang, and J.-F. Chen, "Non-inverting buck–boost converter with interleaved technique for fuel-cell system," *IET Power Electron.*, vol. 5, no. 8, pp. 1379–1388, Sep. 2012.

[25] P. M. García-Vite, C. A. Soriano-Rangel, J. C. Rosas-Caro, and F. Mancilla-David, "A DC–DC converter with quadratic gain and input current ripple cancelation at a selectable duty cycle," *Renew. Energy*, vol. 101, pp. 431–436, Feb. 2017.

[26] N. Zhang, G. Zhang, K. W. See, and B. Zhang, "A single-switch quadratic buck–boost converter with continuous input port current and continuous output port current," *IEEE Trans. Power Electron.*, vol. 33, no. 5, pp. 4157–4166, May 2018.

[27] T.-F. Wu and Y.-K. Chen, "A systematic and unified approach to modeling PWM DC/DC converters based on the graft scheme," *IEEE Trans. Ind. Electron.*, vol. 45, no. 1, pp. 88–98, Feb. 1998.
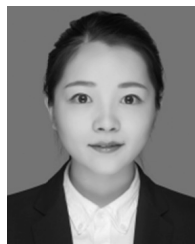
**SHAN MIAO** was born in Shaanxi, China, in 1989. She received the B.S. degree in communication engineering from Northwestern University, Xi'an, China, in 2012, and the Ph.D. degree in electrical engineering from Xi'an Jiaotong University, Xi'an, in 2018. She is currently a Postdoctoral Researcher with the School of Electrical Engineering, Zhengzhou University, Zhengzhou, China.

Her research interests include the construct, modeling, and control of power converter topologies.

**JINFENG GAO** was born in Henan, China, in 1963. He received the B.S. degree in communication engineering, the M.S. degree in electrical engineering, and the Ph.D. degree in electrical engineering from Xi'an Jiaotong University, Xi'an, China, in 1983, 1987, and 2001, respectively. He is currently a Professor with the School of Electrical Engineering, Zhengzhou University, Zhengzhou, China, where he has been involved in research on Nonlinear Circuit Theory, since 1983.

• • •